Volume 5
Number 8
21 April 2021
Pages 2193–2384

Sustainable Energy & Fuels

Interdisciplinary research for the development of sustainable energy technologies

rsc.li/sustainable-energy

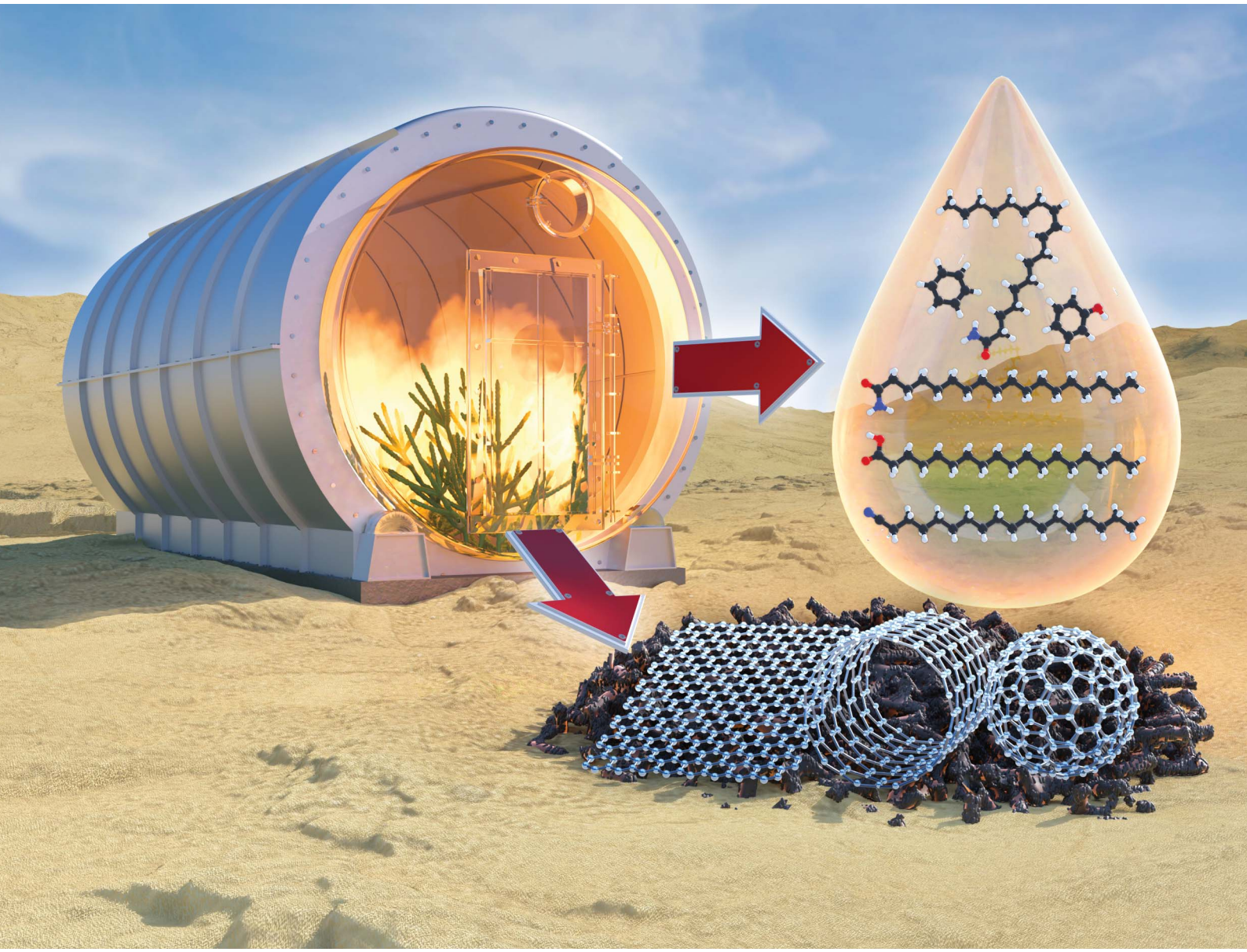

ISSN 2398-4902

ROYAL SOCIETY OF CHEMISTRY

PAPER

Ribhu Gautam *et al.*

Bio-oil and biochar production from halophyte biomass: effects of pre-treatment and temperature on *Salicornia bigelovii* pyrolysis

Sustainable Energy & Fuels

ROYAL SOCIETY OF CHEMISTRY

PAPER

View Article Online
View Journal | View Issue

Check for updates

Cite this: *Sustainable Energy Fuels*, 2021, **5**, 2234

Bio-oil and biochar production from halophyte biomass: effects of pre-treatment and temperature on *Salicornia bigelovii* pyrolysis†

Alessia Iaccarino, Ribhu Gautam * and S. Mani Sarathy

Salicornia bigelovii (SB) is a strategically important plant in many regions owing to its ability to grow in arid climates and saline water. This study evaluates the effects of halophyte biomass pre-treatment on the production of bio-oil and biochar *via* pyrolysis of SB. The pyrolysis experiments were performed in a quartz tube reactor at 600, 700, and 800 °C to understand the effect of the temperature on the products obtained from untreated SB (USB) and pre-treated SB (PSB). USB and PSB samples were characterized to determine their thermal stability, elemental composition, mineral composition, and functional group identification. Pre-treatment of SB reduced the ash and Na content by 71% and 45%, respectively. Ash removal favored the pyrolysis-assisted extraction of carboxylic acids, and their selectivity in the bio-oil increased from 20.7% (USB) to 33.4% (PSB) at 600 °C. The selectivity to phenolics was observed to be the highest at 800 °C in the bio-oil from USB (10.4%) and PSB (13.4%). PSB pyrolysis increased the specific surface area of biochar by four times, whereas carbon nanostructures were observed in the biochar from USB. The formation pathways of the major compounds from the pyrolysis of various amino acids, cellulose, hemicellulose, fatty acids, and lignin present in SB were elucidated by proposing a plausible reaction scheme.

Received 8th November 2020
Accepted 26th February 2021

DOI: 10.1039/d0se01664k

rsc.li/sustainable-energy

Open Access Article. Published on 26 February 2021. Downloaded on 7/28/2024 11:24:34 AM.
This article is licensed under a Creative Commons Attribution-NonCommercial 3.0 Unported Licence.

1. Introduction

The increasing demand for fossil fuel-derived energy has raised the levels of atmospheric greenhouse gas emissions and resulted in widespread concerns about sustainability. Bioenergy can play an essential role in meeting modern-day energy needs with renewable and low environmental impact energy sources.[1] Biomass is recognized as an eco-friendly alternative source of renewable energy and carbon.[2] Based on the method of utilization, biomass can be classified into four categories, *viz.*, first-, second-, third- and fourth-generation. The first generation biomasses are essentially edible crops, whereas second to fourth generation are mainly non-edible.

The use of edible, first-generation biomass crops for the exploitation of energy triggers the food *versus* fuel debate and also increases inflation in food prices.[3] A study published by Rulli *et al.*[4] stated that the amount of food crops utilized to meet bioethanol demand in the top 14 countries was sufficient to feed about 200 million people. Second-generation biomasses are mainly non-edible agricultural or industrial-byproducts.[3] Third-generation biomasses are algal species, whereas fourth-generation biomasses are modified and engineered versions of the first-, second- and third-generation biomasses. The present research to develop fourth-generation biomass is focused on modifying third-generation biomass, for example, algae biomass for enhanced oil production.[5] It is needless to say that the cultivation of first- and second-generation crops requires freshwater and arable land.

Factors such as land and water availability are important from the viewpoint of biomass resource management. Freshwater availability for biomass cultivation is becoming increasingly limited as a result of the rising water demand of the growing world population. Owing to the high salinity levels, every year 1.5 million hectares of land become unsuitable for agricultural production.[6] Therefore, there is a strong need to investigate biomass species which grow in these geographical locations in extreme environments. Halophytes are salt-tolerant plants that represent, at most, 1% of the world's flora. They can grow on marginal soils using saline irrigation water, both of which are unsuitable for conventional crop production.[7] Halophytes are potential oilseeds, forage and biomass crops, and promising carbon sequestration plants.[8] For these reasons, halophytes can be seen as a promising biomass feedstock that can overcome the typical land and water requirements of conventional terrestrial first- and second-generation biomasses.

Salicornia bigelovii is an annual, leafless, and fast-growing halophytic plant.[9] It is considered as one of the most salt-tolerant species among the halophytes, and it can prosper in

Clean Combustion Research Center, Physical Sciences and Engineering Division, King Abdullah University of Science and Technology, Thuwal 23955-6900, Saudi Arabia. E-mail: ribhu.gautam@kaust.edu.sa

† Electronic supplementary information (ESI) available. See DOI: 10.1039/d0se01664k

This journal is © The Royal Society of Chemistry 2021

Open Access Article. Published on 26 February 2021. Downloaded on 7/28/2024 11:24:34 AM.
This article is licensed under a Creative Commons Attribution-NonCommercial 3.0 Unported Licence.

environments with salt concentrations two times greater than that of seawater salinity.[10] Furthermore, unlike many halophytes, its seeds germinate directly on seawater, for this reason, fresh water is not required at any point in the plant's life cycle.[11] The hot and arid climates favor the production of halophytes and their cultivation potential can be understood by considering the world's 22 000 km hot and arid coastline.[12] The prospect of *Salicornia* as a feedstock for conversion has improved as appropriate cultivation techniques can maximize the seed yield to as high as 2 tons per hectare (t ha^{-1}).[13] In 2018, scientists from the International Center for Biosaline Agriculture (ICBA) recorded a significantly high seed yield of 3 t ha^{-1} using seawater in the United Arab Emirates (UAE).[14] The oil yield of SB was found to be higher than that of freshwater oil crops such as soybeans and sunflowers.[15] Also, SB showed a high biodiesel yield (~94%) *via* enzymatic transesterification.[16] The objective of the ICBA is to increase *Salicornia* yields in the UAE and subsequent expansion to the coastal areas of the Arabian Peninsula.[14] As the focus on the cultivation and production of SB is significantly increasing, investigating the potential of SB for energy applications becomes important.

Pyrolysis is a thermochemical decomposition process performed at an elevated temperature (>400 °C) in an inert atmosphere that transforms the biomass into three by-products, *viz.*, a carbon-rich solid (biochar), a liquid fraction (bio-oil) and a gas mixture. Biomass can be converted to chemicals and fuels *via* pyrolysis in a single step. The pyrolysis of terrestrial biomass, as well as aquatic biomass, has been studied in detail.[17,18] However, studies reporting the pyrolysis of halophytes are scarce and focused on the kinetics, detailed information on the pyrolysis products is missing in the currently available literature.[19–22] The growth conditions of these species result in a high mineral content. Therefore, studying the effect of minerals on the pyrolysis products is important for better utilization of these species. A high mineral content in the biomass restricts the scaling-up of the pyrolysis process. Hence, removal of minerals without losing valuable matter from the biomass becomes critical for these types of species. In this study, the characterization of bio-oil and biochar from the pyrolysis of SB is reported in detail. The objectives of this study are threefold: first, to investigate the pyrolysis products from raw and pre-treated SB; second, to study the effect of the temperature on the composition of bio-oil obtained from the pyrolysis of raw and pre-treated SB; and third, to investigate the characteristics of the biochar obtained.

2. Materials and methods

The SB biomass was grown from seeds and harvested in the KAUST greenhouse (22.308381, 39.107794). The biomass was deseeded and only the vegetative portion was utilized in this study.

2.1. Biomass pre-treatment

As a pre-treatment technique, SB was washed with deionized water to reduce the mineral content. First, the SB sample was dried in an oven at 110 °C for 24 h to remove the moisture. Then, the SB sample was ground using a mill grinder (PM200 Retsch). Following this, the sample was mixed with deionized water (1 : 20 w/v) and stirred using a magnetic stirrer at a constant temperature of 25 and 50 °C for a specific duration of 2, 4, 8 and 24 h. After thorough mixing, this solution was vacuum filtered using a Whatman No. 1 filter paper (11 μm). The filter paper was placed on a perforated plate connected to a vacuum pump to enable the liquid to pass through the membrane. The collected SB biomass solids were then dried in an oven at 110 °C for 24 h. After drying, the Na content of the samples was measured using inductively coupled plasma optical emission spectroscopy (ICP-OES, Agilent 5110).

2.2. Characterization of biomass

Both the untreated SB (USB) and pre-treated SB (PSB) were characterized using a thermogravimetric analyzer (TGA), elemental analyzer, ICP-OES, bomb calorimeter to study the thermal stability, elemental composition (C, H, N, S, O), mineral content of ash, and higher heating value (HHV), respectively.

The thermal stability of PSB and USB were investigated using a TGA 5500 (TA Instruments, USA). The TGA experiments were performed with a sample mass of 8 ± 0.5 mg placed in an alumina crucible. The temperature of the sample was raised from ambient temperature to 800 °C at a heating rate of 15 °C min^{-1}. An inert atmosphere was maintained using N_2 at a flow rate of 100 mL min^{-1}. The mass loss and derivative mass loss data were recorded as a function of the time and temperature. Using the same instrument, proximate analyses of PSB and USB were carried out according to the ASTM E 1131-08.[23] The moisture content, and the amount of volatile matter, fixed carbon, and ash were determined. In a typical proximate analysis experiment, 8 mg of the sample was pyrolyzed in an inert atmosphere with an N_2 flow rate of 100 mL min^{-1}. From ambient temperature, the sample was heated (110 °C) and then the mass loss in this regime was recorded as the loss of moisture content. After this, the sample was heated to 900 °C at a heating rate of 80 °C min^{-1}. At this temperature, the sample was held under isothermal conditions and the mass loss registered was recorded as volatile matter. The N_2 in the system was switched to air at the same flow rate of 100 mL min^{-1}. The sample was maintained isothermally at 900 °C for 45 min and the final amount of the sample remaining was noted as ash content. Finally, the fixed carbon content was determined from the difference, for example, fixed carbon wt% = 100 − moisture wt% − volatile matter wt% − ash wt%.

The elemental composition (CHNS) of the samples was determined using a Thermo Flash 2000 (Thermo Fisher Scientific, U.S.A.) organic elemental analyzer. A sample mass of 2.5–3 mg was used in this type of experiment. The typical construction of an elemental analyzer consists of a combustion tube. This combustion tube was heated to around 1000 °C in the presence of air. The elements, *viz.*, carbon, hydrogen, nitrogen, and sulfur, present in the sample were converted to their respective oxides. The vapors evolved from the combustion of the sample were passed through a gas chromatography/thermal

Open Access Article. Published on 26 February 2021. Downloaded on 7/28/2024 11:24:34 AM.
This article is licensed under a Creative Commons Attribution-NonCommercial 3.0 Unported Licence.

conductivity detector (GC/TCD). The GC/TCD was pre-calibrated for the determination of carbon, hydrogen, nitrogen, and sulfur content. It is worth mentioning that the nitrogen oxides were reduced to N_2 using a Cu based catalyst before the vapors were analyzed in the GC/TCD system. The oxygen content was calculated using the difference (O% = 100-ash% -C% -N% -H%).

The mineral content (Al, Ca, Na, Mg, Si and Fe) of the samples was determined using an Agilent ICP-OES 5110. Before these experiments were performed, the samples were digested in acid and then subjected to microwave treatment in an SRC system (UltraWave™, Milestone, Sorisole, Italy).

The higher heating values of both the samples were determined in an isoperibolic (constant temperature surroundings) calorimeter (Parr 6400). In a typical bomb calorimetry experiment, 0.5 g of dried sample is placed in a stainless steel cup and then placed in the calorimeter for combustion. For the estimation of HHV, it is assumed that the condensation of water vapors produced takes place completely. The value given by the instrument is taken directly as the HHV of the sample in MJ kg^{-1}. All the experiments were repeated non-consecutively to establish confidence in the experimental data.

2.3. Experimental setup: pyrolysis reactor

The pyrolysis experiments were performed in a customized reactor. A schematic diagram of the reactor is shown in Fig. 1. The major components of this reactor were as follows: supply line for inert gases, flowmeter, thermocouple, reactor chamber, condenser, bio-oil trap, and discharge line for gaseous products. The reactor chamber consisted of a quartz tube (21 mm i.d., 25 mm o.d, and 520 mm in length) with stainless steel fittings for the gas inlet and exit, respectively. The reactor chamber was placed in an electrically heated CY-O1200-50ICS tube furnace (CY Scientific Instrument, China). A thermocouple (OMEGA HH802-U) was also inserted through an access provided in the tube furnace to record the temperature in the furnace. The temperature of the furnace was regulated using a proportional integral derivative controller which allows an extensive range of heating rates and hold times with a possible high treatment temperature (HTT) of over 1000 °C. Fig. 2 represents the temperature profiles observed across the length of the furnace. These profiles were obtained by fixing the different pyrolysis temperatures, *viz.*, 600, 700, and 800 °C and placing the thermocouple at different positions in the quartz

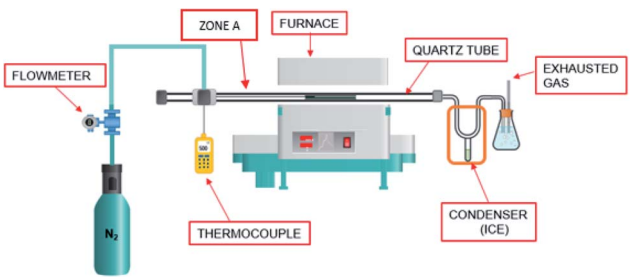

Fig. 1 Schematic diagram of the pyrolysis reactor used in this study.

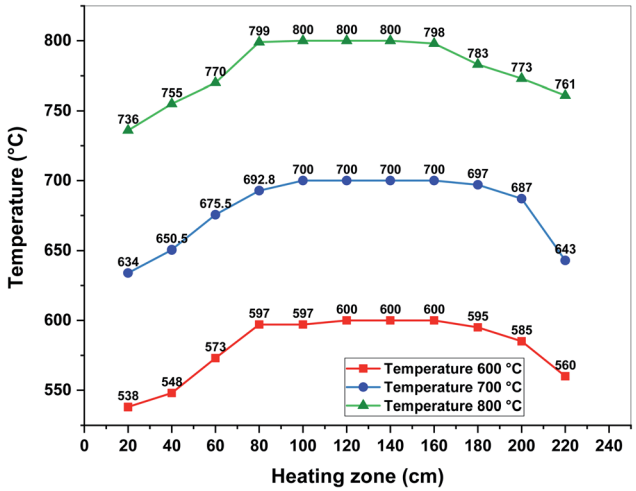

Fig. 2 Measured temperature profiles at different pyrolysis temperatures across the length of the quartz tube.

reactor. The central area, approximately 100 mm in the reactor, was observed to maintain the set pyrolysis temperature. The inlet and outlet areas had significant temperature gradients that had high temperatures so as to avoid the condensation of the vapors. Also, the furnace was jacketed to ensure the operator's safety.

The reactor was purged with N_2 for 10 min to maintain the inert environment before each experiment. For a pyrolysis experiment, the dried biomass sample was placed in a steel tube closed at the outlet with a steel mesh to confine the biomass. Initially, the steel tube containing the biomass sample was placed in the quartz tube, so that it was outside the furnace (in Zone A) as shown in Fig. 1. When the furnace reached the desired pyrolysis temperature, the metal tube was pushed inside the furnace. It was ensured that the position of the steel tube with the sample was in the central area, the zone in which the temperature was the same as the set pyrolysis temperature. At the reactor outlet, the gases passed through a condenser immersed in ice. In the downstream from the condenser, the condensable fraction was collected in a stainless steel tube blinded with a Swagelok blind nut. The flow of exhaust gases was passed through a plastic tube leading to the fume hood.

The pyrolysis experiments were conducted at temperatures, *viz.*, 600, 700, and 800 °C with USB and PSB. A continuous flow rate of N_2 was kept at 100 mL min^{-1} to maintain the inert atmosphere and to sweep away the pyrolysis vapors. The sample mass of approximately 15 g was taken in the steel tube before placing it in the quartz tube reactor. The temperature of the tube furnace was ramped at 10 °C min^{-1} from ambient temperature to the desired pyrolysis temperature. Before pushing the steel tube into the Zone A, the setup was allowed to settle for 30 min. The steel tube was then pushed inside and placed in the Zone A. The residence time, which was 20 min for the pyrolysis, was decided on the basis of completion of the pyrolysis of the biomass. The furnace was switched off after the pyrolysis was complete and the steel tube was pushed out of the furnace for cooling under the same nitrogen flow. This cooling

Open Access Article. Published on 26 February 2021. Downloaded on 7/28/2024 11:24:34 AM.
This article is licensed under a Creative Commons Attribution-NonCommercial 3.0 Unported Licence.

made sure that no undesired combustion of char took place and also the absorption of moisture was avoided. For accurate determination of the bio-oil yield, the condenser system used for the collection of bio-oil was weighed before and after the experiment. Finally, the collected biochar and bio-oil were weighed *via* gravimetry.

It is worth mentioning that the percentage mass yields of the biochar and bio-oil were calculated on a dry basis. The ratio between the mass of the produced biochar and bio-oil and the mass of the feedstock, *viz.*, USB and PSB, were used to calculate the yields as given in eqn (1) and (2).

$$Y_{\text{biochar}}(\%) = \frac{M_{\text{biochar}}}{M_{\text{feed}}} \times 100 \quad (1)$$

$$Y_{\text{bio-oil}}(\%) = \frac{M_{\text{bio-oil}}}{M_{\text{feed}}} \times 100 \quad (2)$$

In eqn (1) and (2), M_{biochar}, $M_{\text{bio-oil}}$ and M_{feed} represent the mass of the biochar, bio-oil, and USB and PSB feedstock, respectively. Y_{biochar} and $Y_{\text{bio-oil}}$ are the percentage yields of biochar and bio-oil, respectively.

2.4. Gas chromatography/mass spectrometry analysis of the bio-oil

The bio-oil samples obtained from USB and PSB at different temperatures were collected. Typically, bio-oil is composed of organics and water. The organic composition of the bio-oil was analyzed using gas chromatography/mass spectrometry (GC/MS). Dichloromethane (HPLC grade) was used in the ratio of 4 : 1 (v/v) to dilute the bio-oil prior to injection into the GC/MS. 1 μL of diluted bio-oil was injected into the GC/MS (Agilent 7890A GC-5975C MSD). The sample was injected at 300 °C and the bio-oil vapors were separated in an Agilent DB-5MS capillary column (60 m length × 0.25 mm i.d. × 0.10 mm in thickness). The bio-oil vapors were carried using ultrahigh pure helium (99.9995%) at a column flow rate of 2 mL min^{-1} and a split ratio of 10 : 1. The GC oven was kept at 40 °C initially for 1 min and then the temperature was ramped at a heating rate of 10 °C min^{-1} to 300 °C. Finally, the oven was kept at this temperature for 26 min. The temperature of the GC/MS interface was maintained at 300 °C. The EI (electron ionization) potential of the ion source in the MS was 70 eV and the detector temperature was maintained at 250 °C. The separated compounds present in the bio-oil vapors were scanned in the *m*/*z* range of 35–700 Da. The separated compounds were identified by comparison of the mass spectra of the compounds with the existing NIST and Wiley libraries. The compounds with match factors above 85% were considered in the analysis and the abundance of the compounds was reported as the relative peak area percentage. The relative peak area percentage can also be proportional to the selectivity percentage. More than 300 different compounds were identified in the bio-oil, therefore quantification based on the calibration of pure compounds was not performed in this study.

2.5. Characterization of biochar

The biochar obtained from the pyrolysis of USB and PSB at different temperatures was characterized in detail *via* an elemental analyzer, pH meter, conductivity meter, Fourier transform infrared spectroscopy (FTIR), Brunauer–Emmett–Teller (BET) porosimetry and scanning electron microscopy (SEM) coupled with energy-dispersive X-ray spectroscopy (EDX). The elemental analysis of the biochar obtained was performed as per the procedures employed for the USB and PSB biomass samples. The pH and electrical conductivity were measured by preparing the suspension of different biochar samples in Milli-Q water with a concentration of 10% (w/v). The suspension was prepared by mixing the biochar in the water for 2 h at 25 °C. The pH was measured in a Mettler Toledo pH meter and the electrical conductivity was measured using a Mettler Toledo Orion 5-Star Benchtop Multiparameter Meter.

The functional groups present in the biochar samples were investigated using a Thermo Scientific Nicolet iS10 FTIR spectrometer (Thermo Fisher Scientific Inc., USA) operated in the attenuated total reflectance (ATR) mode. The biochar samples were spread over the diamond crystal and it was ensured that the crystal was completely covered with the sample. The FTIR spectra of the biochar samples were collected in the wavenumber region 4000–750 cm^{-1} at a resolution of 2 cm^{-1}. The surface area measurements of biochar samples were performed in an ASAP 2420 (Accelerated Surface Area and Porosimetry) system (Micrometrics Instrument Corp., USA). Before the porosimetry experiments, the biochar samples were degassed at 120 °C for 3 h under vacuum. The degassing phase is intended to remove the gas, humidity or volatile compounds present inside the porous structure of the biochar, which may alter the adsorption tests. The surface area was measured using the BET nitrogen gas physisorption method at 77 K over a relative pressure range of P/P_0 = 0.01–0.99. To probe the surface morphology of various biochar samples, experiments were performed using a Zeiss Merlin SEM coupled with the Oxford Instrument EDX. These analyses investigated the nanoscale morphologies of biochar. During the analyses, the high electron tension and probe current were set to be 5 keV (maximum) and 2 pA, respectively, to prevent possible destruction to carbon black. An appropriate working distance and the beam focus were adjusted accordingly to obtain a high-resolution image. The ash content in the biochars was determined from the mass of the residues obtained after the samples were heated to a controlled temperature of 550 ± 10 °C according to standards provided in EN 1SO 18122:2015. The mineral content of ash was also determined using ICP-OES.

3. Results and discussions

3.1. Biomass pre-treatment

The SB biomass was pre-treated by washing in water and the effects of the parameters such as the washing time and the temperature were investigated. This aided in establishing optimal conditions for biomass pre-treatment. Water-washing is seen as a simple and promising pre-treatment technique

Open Access Article. Published on 26 February 2021. Downloaded on 7/28/2024 11:24:34 AM.
This article is licensed under a Creative Commons Attribution-NonCommercial 3.0 Unported Licence.

for removal of the large amounts of minerals present and improving the pyrolysis and combustion characteristics.[24] Blasi *et al.*[25] also observed more than 50% ash removal using water-washing of straw. Water-washing has shown promising results in the removal of Na and K from the matrix of biomass. Cen *et al.*[26] observed metal removal efficiencies from rice straw in the range of 75–80% for Na and K. It can be noted that the water-washing did not result in significant ash removal, which is in contrast to the reduction in the ash content reported in this study. In recent studies, washing of the rice straw with the aqueous phase of bio-oil led to very high metal removal efficiencies (~99% for Na and K).[26,27] Readers can refer to comprehensive reviews published by Kumar *et al.*[28] and Putro *et al.*[29] for various pre-treatment techniques to produce drop-in fuels and valuable chemicals, respectively, from lignocellulosic biomasses.

Water-washing primarily resulted in the demineralization of the SB biomass. The Na content of the untreated biomass was observed to be 10.28%. Fig. S1 (in the ESI†) depicts the effect of the time and temperature on the Na content of SB. It can be seen from Fig. S1† that the Na content reduced gradually with the duration of the treatment at both temperatures, *viz.*, 25 and 50 °C. Deng *et al.*[24] also studied the effect of the water temperature on the removal of potassium and chlorine between 30–90 °C. It is important to note that increasing the pre-treatment temperature from 25 to 50 °C significantly enhanced the Na reduction in the range of 16–28% across all washing times. This effect can be attributed to the enhanced solubility of the minerals in the washing medium at higher temperatures. In addition, there is a possibility of opening the biomass matrix in the presence of hot water. This opening allows the deeper penetration of the washing medium within the biomass particles and hence the increased removal of inorganic matter is observed. Based on these results, the optimum washing conditions were found to be 8 h of treatment at 50 °C. The Na content was 5.65% under optimized pre-treatment conditions. Furthermore, the Ca content decreased from 2.40% (USB) to 0.64% (PSB). Longer washing times did not offer significantly improved demineralization.

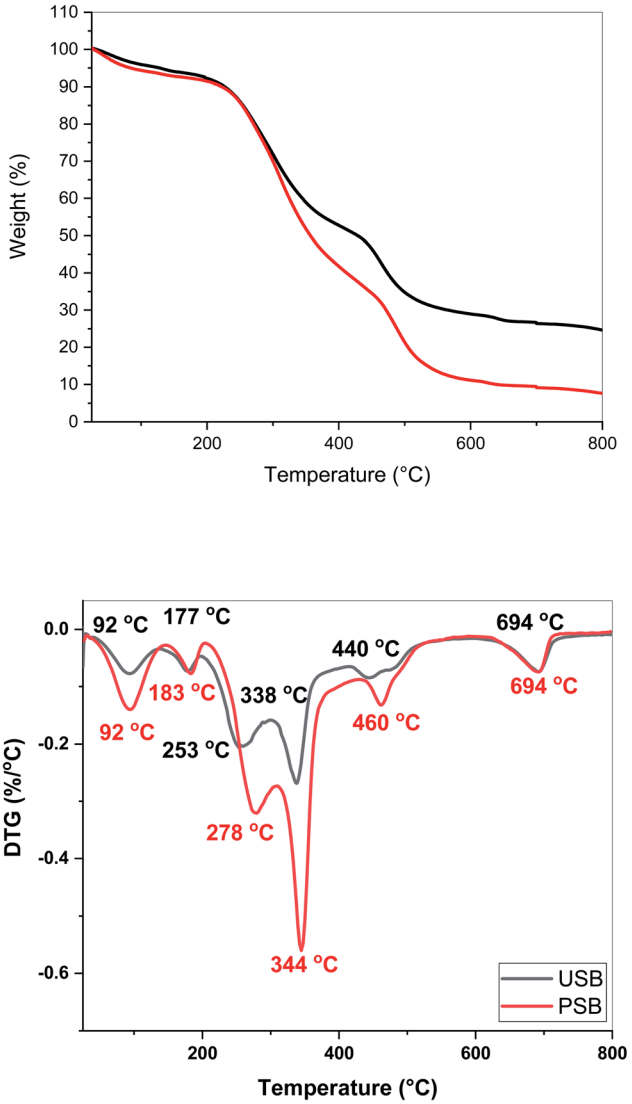

Fig. 3 Thermogravimetric (top) and differential thermogravimetric profiles of USB and PSB acquired at 15 °C min^{-1}.

3.2. Characterization of the biomass

Fig. 3 depicts the thermogravimetric and differential thermogravimetric (DTG) profiles of the USB and PSB. T_m, mentioned in the DTG profiles, denotes the temperature at which the maximum mass loss rate was recorded. T_m was also used to identify the decomposition regimes of the different biochemical components present in the SB. Various T_m values are represented using color in the respective DTG profiles of USB and PSB to give a better understanding of the decomposition of the various components of SB. The multiple peaks observed in the DTG profile clearly indicate the presence of more than one component and the involvement of the multi-step thermal decomposition during the pyrolysis of SB.

From the TG curves, the major decomposition of both USB and PSB occurred in the temperature range of 200–500 °C. The similarity in the decomposition of USB and PSB can be attributed to the similar constituents in the matrix of the biomass, irrespective of the pre-treatment. As expected, the final residue observed for PSB was significantly lower than for USB. This can be attributed to the removal of the minerals during the pre-treatment of the SB. The mass loss observed up to 150 °C was due to the moisture physically bound to the biomolecules of the SB. Therefore, $T_m = 92$ °C represents the release of the water from the biomass. The mass loss in the range of 150–200 °C was due to the release of the low-molecular weight compounds. The peaks in the region 250–280 °C were due to the decomposition of the hemicellulose present in the SB.[21,30] The onset of the decomposition of cellulose was around 250 °C, this peak also represented the portion of cellulose decomposing in this temperature range.[31] As amino acids are present in the matrix of the SB biomass, the decomposition regime between 300–350 °C can be attributed to the decomposition of the cellulose, as well as the proteins.[31–33] SB biomass also contains carboxylic acids,

 This journal is © The Royal Society of Chemistry 2021

Open Access Article. Published on 26 February 2021. Downloaded on 7/28/2024 11:24:34 AM.
This article is licensed under a Creative Commons Attribution-NonCommercial 3.0 Unported Licence.

such as palmitic and linoleic acids, present in the matrix.[32] The peak around 450 °C can be attributed to the decomposition of lipids, which have carboxylic acids as the backbone.[33] The last peak is observed at 694 °C in both the USB and PSB. To ascertain the presence of this peak, TGA experiments were performed multiple times. A similar peak around 700 °C was also observed in the DTG of *Salicornia bigelovii* and reported by Dzidzienyo *et al.*[21] This may be attributed to the decomposition of the lignin fraction present in SB. This is in line with the results obtained in previously reported literature, as lignin exhibits decomposition at higher temperatures up to 900 °C.[31,34]

Table 1 shows the proximate analyses of USB and PSB and the representative percentages by weight of moisture, volatile matter, ash and fixed carbon. The ash content of PSB was found to be significantly lower (7.1 wt%) than USB (24.2 wt%). This observation was in line with the TGA profiles obtained, considering the fixed carbon content of the USB and PSB. The pre-treatment of SB with water reduced the ash content significantly. This clearly indicates that part of the mineral content that was lost constituted water-soluble components such as nitrates, carbonates, chlorides, and phosphates, as observed for terrestrial biomass.[35] The role played by minerals in the pyrolysis of the biomass component, cellulose, was previously reported by Brown and coworkers.[36] They studied the effect of inorganic salts such as NaCl, KCl, $MgCl_2$, and $CaCl_2$ on the primary pyrolysis products. The volatile fraction of PSB (85%) was more than that of USB (69%). This increase can be attributed to the removal of minerals from the matrix of the SB.

The elemental (C, H, N, S, O) composition of USB and PSB are presented in Table 1. The nitrogen content in both the samples can be attributed to the presence of various amino acids. As the volatile composition of PSB was more than USB, this translated to the enhanced carbon content of PSB (50.7 wt%) as compared to USB (35.5 wt%). This increase in the carbon content and significant ash removal resulted in an increase in the HHV from 10.2 MJ kg^{-1} (USB) to 17.6 MJ kg^{-1} (PSB). As compared to other fossil fuels, such as petroleum-based fuels and coal, the carbon and oxygen content were low and high, respectively.[37] The source of oxygen in the SB is primarily the cellulose, hemicellulose, lignin, and carboxylic acid backbone present in the matrix.

The Al, Ca, Fe, Mg, Na and Si content of USB and PSB were determined using ICP-OES and are tabulated in Table 2. For PSB, the case using the optimum parameters (50 °C, 8 h) was selected for the determination of the minerals *via* ICP-OES. The mineral content of biomass is present on the particle surface because of contact with soil during harvest and/or transportation, or within the material as biogenic characteristics. In SB, Na^+ is stored in the vacuoles.[38] It can be seen from Table 2 that Na is the primary inorganic in the plant mineral composition. The pre-treatment process significantly removes the metals and the quantities of all the identified metals decreased in PSB. It should be noted that a significant fraction of the alkali and alkaline earth metal (AAEM) species showed a reduction of about 50%. A significant quantity of calcium was removed in comparison with the other elements. It is important to highlight that the main contribution to fouling, scaling deposits, slagging and corrosion comes from the inorganic part of the biomass.[39] By employing this pre-treatment technique, the discussed issues, which are bottlenecks for the scaling up of SB biomass pyrolysis, can be addressed. These metals, present in the matrix of the biomass, assume an important role in deciding the composition of the pyrolysis bio-oil and biochar, as discussed later.

Table 2 Mineral content (wt%) in USB and PSB used in this study (dry basis)

	Al	Ca	Fe	Mg	Na	Si
USB	0.20%	2.40%	0.20%	0.72%	10.28%	0.16%
PSB	0.07%	0.64%	0.05%	0.18%	5.65%	0.1%

3.3. Pyrolysis of SB

3.3.1. Effect of temperature and pre-treatment on product yields. Fig. 4 depicts the effect of temperature on the pyrolytic yields from USB and PSB. The bio-oil and biochar fractions are only accounted for in the final products. It should be noted that the focus of the present study is to understand the effect of minerals and temperature on the bio-oil composition and properties of biochar. The fractional bio-oil yield from the pyrolysis of USB increased from 0.181 at 600 °C to 0.252 at 700 °C before decreasing to 0.208 at 800 °C. The bio-oil yield increased from 600 °C as compared to 700 °C owing to reactions such as thermal cracking and dehydration, resulting in the enhanced formation of volatiles. Beyond 700 °C, the bio-oil yield decreased owing to the cracking of the volatiles into non-condensable gases such as CO_2, CO, and CH_4. These observations, an increase and then a decrease in the bio-oil quantity, were in line with the literature on biomass pyrolysis.[40–42] The fractional yields of biochar gradually decreased as a function of

Table 1 Characteristics of USB and PSB used in this study. The values are in wt% and the data are presented as the mean ± S.D., $n = 3$[a]

	Proximate analysis (air dried basis)					Elemental analysis (dry basis)					
	Moisture (%)	Volatile matter (%)	Fixed carbon (%)	Ash (%)	HHV (MJ kg^{-1})	C (%)	H (%)	N (%)	S (%)	O (%)	H/C	O/C
USB	4.4 ± 0.9	68.9 ± 0.2	2.5 ± 0.0	24.2 ± 0.9	10.18 ± 0.6	35.53 ± 1.4	5.53 ± 0.6	2.80 ± 0.2	1.08 ± 0.1	31.95 ± 0.4	1.85	0.63
PSB	6 ± 0.6	84.8 ± 2.0	2.1 ± 1	7.1 ± 0.8	17.57 ± 0.7	50.74 ± 1	7.4 ± 0.1	4.65 ± 1	1.1 ± 0.12	22.65 ± 0.3	1.73	0.42

[a] % C + % H + % N + % O + % Ash = 100.

Open Access Article. Published on 26 February 2021. Downloaded on 7/28/2024 11:24:34 AM.
This article is licensed under a Creative Commons Attribution-NonCommercial 3.0 Unported Licence.

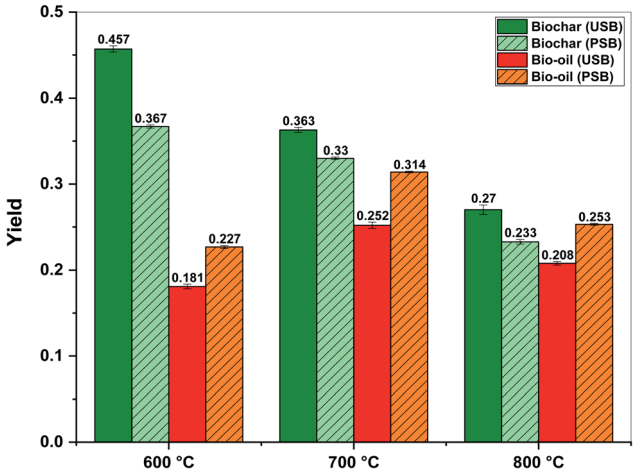

Fig. 4 Effect of temperature on the yields of the pyrolysis products from USB and PSB.

the temperature and followed the trend: 0.457 (600 °C) > 0.363 (700 °C) > 0.270 (800 °C). This can also be attributed to the enhanced cracking of the organic matter. The bio-oil yield combined with the char yield at 800 °C indicated the enhanced gas fraction.

From Fig. 4, it can be observed that the pre-treatment of SB resulted in a significant increment in the bio-oil yields across all the pyrolysis temperatures. The fractional bio-oil yields from the pyrolysis of PSB increased from 0.227 at 600 °C to 0.314 at 700 °C before decreasing to 0.253 at 800 °C. The biochar yields from the pyrolysis of PSB followed the trend: 0.367 (600 °C) > 0.33 (700 °C) > 0.233 (800 °C). The pre-treatment of SB increased the conversion with respect to biochar in the range of 9.1–19.7% across the three pyrolysis temperatures. The reduced char yields can be attributed to the cracking of heavy hydrocarbons in the biomass, as cracking increased with the increase in temperature. Also, the formation of primary char was successively less favored as compared to the volatiles formed. Consequently, there is an enhancement in the production of liquid and gaseous products. The role of the AAEM species in the pyrolysis process cannot be neglected and it is important to mention that the removal of these species reduced the biochar yields. In the case of biomass pyrolysis, the AAEM species promote the charring reaction, which leads to the formation of secondary char.[43] The presence of the AAEM species is also capable of inhibiting the vapor cracking reactions, resulting in the formation of gas and water from pyrolysis.[44] This effect translated into enhanced gas formation from the pyrolysis of PSB. This can be assumed from the values of the bio-oil and biochar as actual gas yields were not recorded.

For USB as well as PSB, the optimum pyrolysis temperature concerning the bio-oil yield was 700 °C. Overall, the low bio-oil and biochar yields at a higher temperature are attributed to the secondary decomposition of the char and pyrolysis vapors. The pre-treatment of SB increased the bio-oil yield by 24.6% as compared to the bio-oil yield from USB at 700 °C. The bio-oil yields from the pyrolysis of pre-treated biomass at 600 and 800 °C also significantly increased by 25.4% and 21.6%, respectively, as compared to untreated biomass. These increased bio-oil yields from the pyrolysis of PSB can certainly be attributed to the increased volatile fraction (~69% to 85%) and the reduced ash content (~24% to 7%). Several studies have demonstrated the positive effects of lower bulk ash content on the liquid yields during thermochemical processes.[42,44]

3.3.2. Composition of the bio-oil from the pyrolysis of USB.

The bio-oil obtained from the pyrolysis of USB and PSB at different temperatures significantly varied in composition. In this section, the effect of temperature on the composition of the bio-oil was investigated. It is concluded from the previous section that the removal of AAEM species affected the product yields. The compounds present in the bio-oil were classified broadly into the following categories, *viz.*, aliphatic hydrocarbons, aromatic hydrocarbons, carboxylic acids, amines/amides, cyano/nitriles, N-aromatic compounds and phenolics. The different components present in SB can be related to different compounds in the bio-oil. The vegetative portion of SB has the characteristics of typical lignocellulosic biomass. The cellulose, hemicellulose and lignin were in the range of 45–47 wt%, 14–15 wt% and 1.5–2 wt%, respectively in the SB.[45] Proteins and fatty acids are also present in the biomass matrix.[32] The major amino acids present in SB are proline, asparagine, lysine, glutamic acid, phenylalanine and leucine.[32] Palmitic acid and linoleic acid are the major fatty acids present.[32] The presence of fatty acids in our bio-oil confirms the presence of fatty acid esters in SB.

Fig. 5 shows the composition of the major types of compounds in bio-oil obtained from the pyrolysis of USB at different temperatures. Carboxylic acids were significantly present in the bio-oil (10–21 area%) obtained from the pyrolysis of USB at different temperatures. The trend, followed by the selectivity to carboxylic acids in the bio-oil, was as follows: 20.70% (600 °C) > 12.90% (700 °C) > 10.28% (800 °C). This can be attributed to the decarboxylation and cracking of carboxylic acids as the pyrolysis temperature increases. The selectivity to *n*-hexadecanoic acid was 13.85% at 600 °C, which decreased to

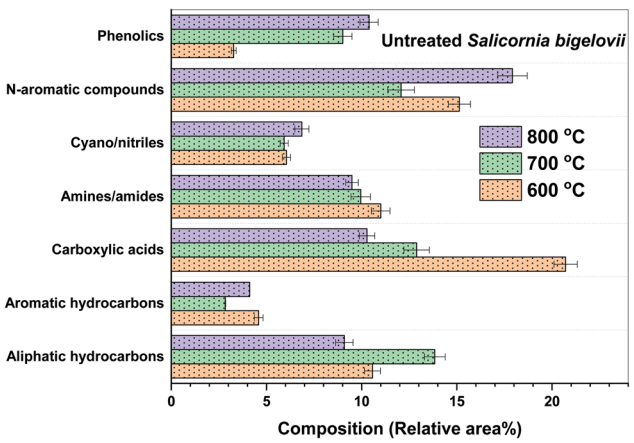

Fig. 5 Effect of temperature on the composition of bio-oil from the pyrolysis of USB.

This journal is © The Royal Society of Chemistry 2021

Open Access Article. Published on 26 February 2021. Downloaded on 7/28/2024 11:24:34 AM.
This article is licensed under a Creative Commons Attribution-NonCommercial 3.0 Unported Licence.

6.43% at 700 °C and finally reduced to 5.74% at 800 °C. The selectivity to linoleic acid followed the trend: 6.3% (600 °C) > 4.83% (700 °C)–4.22% (800 °C). As these fatty acids were present in the matrix of SB, it can be noted that these are not pyrolysis products. The high temperatures employed in pyrolysis aided in their extraction into the bio-oil. Similar extraction of fatty acids from the lipids present in different algae species was also observed during pyrolysis.[41,46] This clearly suggests the pyrolysis-assisted extraction of fatty acids from the matrix of the biomass. Carboxylic acids such as methyl butanoic acid, octanoic acid and decanoic acid were also present in traces in the bio-oil. These acids were a result of cracking of long chain fatty acids. Aliphatic hydrocarbons were also present in considerable amounts and these were primarily produced from decarboxylation of carboxylic acids along with the production of carbon dioxide. The selectivity to the aliphatic hydrocarbons was 10.5% at 600 °C which increased to 13.84% (700 °C) and then decreased to 9.1% at 800 °C. This decrease in the amount of aliphatic hydrocarbons can be linked to cracking at high temperatures resulting in the conversion of volatiles into non-condensable gases such as CO_2 and lighter hydrocarbons. Scheme 1 depicts the plausible reactions of the different components of SB under pyrolysis conditions, producing various compounds.

The nitrogen content in USB is higher (2.8 wt%) than that in other terrestrial lignocellulosic biomass.[42–44] The nature of the proteins played a role in the formation of various nitrogen-containing compounds. For example, glutamic acid is an amino acid with two C=O linkages, asparagine is an amino acid with two $-NH_2$ and two C=O linkages, phenylalanine consists of a benzene ring and proline has a five-membered ring with nitrogen lodged in the ring. These amino acids resulted in the formation of N-aromatic compounds, which were major nitrogen-containing heterocyclic compounds, cyano/nitriles, and amines/amides. The selectivity to the N-aromatic compounds was highest in the bio-oil obtained at 800 °C (17.92%) followed by 15.13% at 600 °C and 12.07% at 700 °C. The high amounts of N-aromatic compounds at 800 °C can be attributed to the enhanced cyclization and aromatization reactions at high pyrolysis temperatures. Many important nitrogen containing platform chemicals were observed in the bio-oil such as 1H-pyrrole, 2-methyl pyrazine, 1H-indole, 2,4-imidazolidinedione, 2-pyrrolidinone and 3-pyridinol. The amino acids undergo decarboxylation and cyclization to produce compounds such as 3,4-dimethyl benzene, *N*,*N*-dimethyl methanamine and *N*,*N*,4-trimethyl benzenemethanamine. These compounds were observed in the bio-oil and undergo successive hydrogen removal to produce benzenepropanitrile and benzylnitrile. These reactions are also evidenced in the literature concerning the pyrolysis of amino acids.[47] The amino acids underwent other reactions such as dehydration reactions to produce important compounds such as aminopyrimidine, 2-

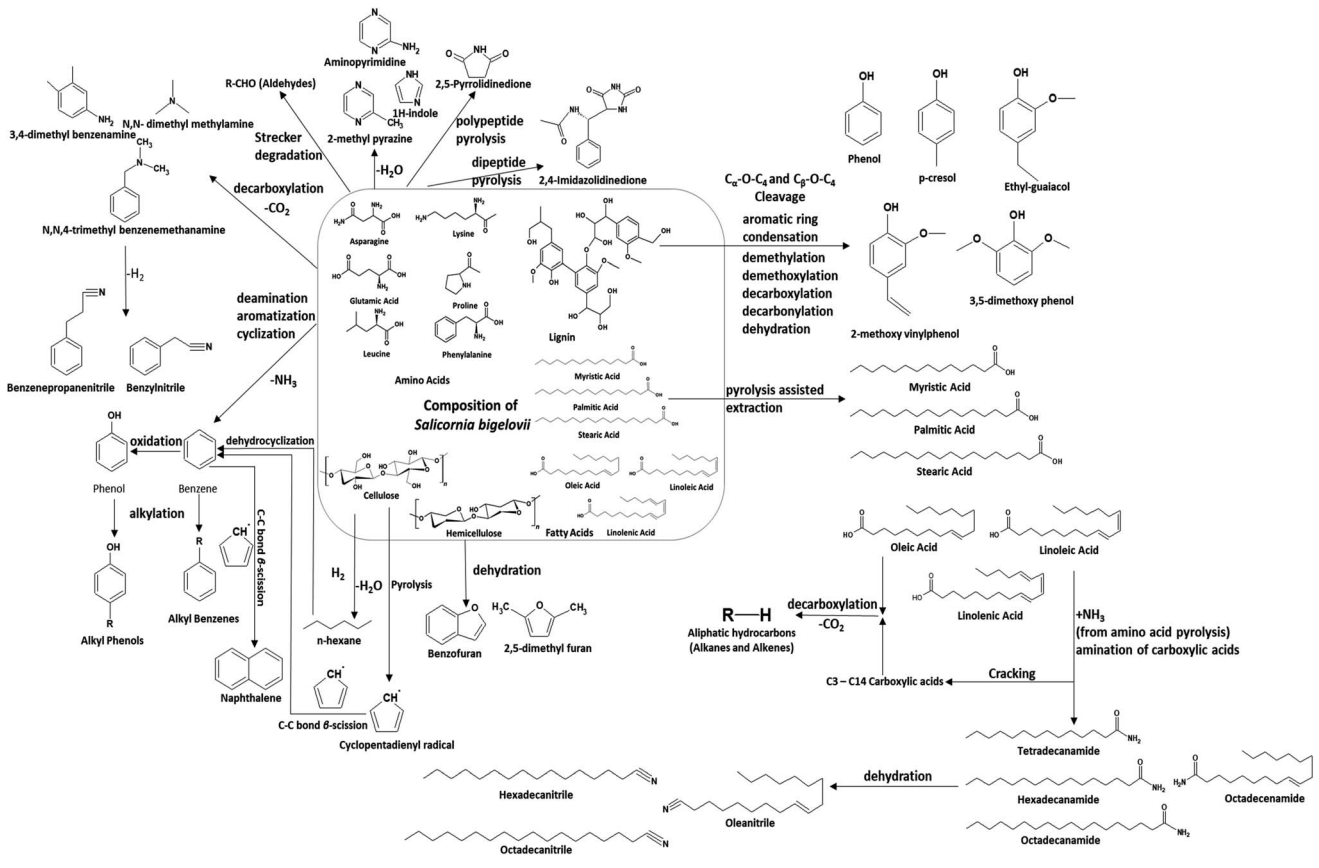

Scheme 1 Plausible reactions occurring during pyrolysis of *Salicornia bigelovii*.

Open Access Article. Published on 26 February 2021. Downloaded on 7/28/2024 11:24:34 AM.
This article is licensed under a Creative Commons Attribution-NonCommercial 3.0 Unported Licence.

methyl pyrazine and 1H-indole. Pyrolysis of the polypeptides present in amino acids led to the production of 2,5-pyrrolidinedione derivatives, whereas pyrolysis of dipeptides resulted in the formation of 2,4-imidazolidinedione derivatives.[47] A discussion on the production of these compounds is important as these are abundantly present in the bio-oil obtained from the pyrolysis of SB.

The different biochemical compounds present in the matrix of SB relate to the different categories of compounds. Therefore, interactions between the compounds from different biochemical components are also possible. Amino acids during pyrolysis undergo deamination which results in the evolution of ammonia. This ammonia interacts with carboxylic acids to form carboxylic acid amides or fatty amides. The selectivity of the fatty amides marginally decreased from 10.1% (600 °C) to 9.2% (700 °C) and finally to 8.81% at 800 °C. Major fatty amides present in the bio-oil obtained at different temperatures were hexadecanamide, 9-octadecenamide, *N*,*N*-dimethyl 9-octadecenamide, *N*-methylhexadecanamide and *N*,*N*-dimethylpalmitamide. These amides dehydrate during pyrolysis to produce nitriles. Pentadecanenitrile, heptadecanenitrile and oleanitrile were the major nitriles obtained from the dehydration of fatty amides. At 800 °C, significant cracking of nitriles can be justified by the presence of acetonitrile, propanenitrile and 4-methyl pentanenitrile. The overall selectivity to the nitriles/cyano compounds in the bio-oil was found to be 6–7% for all the pyrolysis temperatures. Amides and nitriles are important from the point of view of applications in pharmaceutical ingredients.

The presence of low-molecular weight carbonyl compounds (aldehydes and ketones) and furan derivatives were a result of the presence of cellulose and hemicellulose in the SB biomass. Levoglucosan is a primary product obtained from the pyrolysis of cellulose.[36] The pyrolysis temperatures and residence time of the vapors in this study facilitated the secondary reactions and conversion of levoglucosan into other low-molecular weight oxygenates and non-condensable gases. The dehydration of cellulose results in the formation of furan derivatives, such as 3-dodecyl 2,5-furandione, 1-(2-furanyl)-ethanone, 2-furanmethanol, 1-(2-furanyl)-2-hydroxy-ethanone and 5-ethyl-2-furaldehyde. The decomposition of hemicellulose resulted in the formation of polycyclic compounds, and benzofuran derivatives, such as 2,3-dihydro-benzofuran. The selectivities to furan derivatives in the bio-oil were 1.66%, 1.52% and 1.55% at 600, 700 and 800 °C, respectively. The selectivity to carbonyl compounds increased with the increase in temperature as follows: 2.16% (600 °C) < 4.77% (700 °C) < 5.63% (800 °C). The major ketones observed in the bio-oil contained a 2-cyclopenten-1-one backbone which are typical pyrolysis products from cellulose, as well as hemicellulose.[36,48] The content of ketones was found to increase with the temperature, which is in line with results previously reported in the literature.[48] The pyrolysis products from cellulose and hemicellulose in the bio-oil were similar to those found from pyrolyzing pure cellulose and hemicellulose in a tube reactor.[48]

Phenolic compounds in the bio-oil were present in noticeable amounts. These compounds were a result of primarily lignin pyrolysis, as it is a biopolymer consisting of phenylpropanoid monomers through C–O and C–C linkages.[48,49] The selectivity to phenolics increased significantly with temperature as follows: 3.28% (600 °C) < 9% (700 °C) < 10.4% (800 °C). The major phenols were *p*-cresol and 2-methoxy phenol. Lignin deconstruction takes place *via* reactions such as C_α–O–C_4 and C_β–O–C_4 cleavage, aromatic ring condensation, demethylation, demethoxylation, decarboxylation, decarbonylation and dehydration.[49] The formation of phenols also took place from the pyrolysis of amino acids such as phenylalanine.[47] Phenolics were also responsible for the production of aromatic hydrocarbons *via* deoxygenation, as shown in Scheme 1.

Aromatic hydrocarbons were present in the bio-oil and their selectivity was in the range of 2.8–4.6% at all the three pyrolysis temperatures. Toluene and xylene were noticeable aromatic hydrocarbons present in the bio-oil. Apart from the deoxygenation of phenols, a minor amount of aromatic hydrocarbons can be formed from cellulose. The presence of the cyclopentadiene fraction in the bio-oil composition ascertains the formation of the cyclopentadienyl radical. Traces of polycyclic aromatic compounds, such as naphthalene and its derivatives, were also present in the bio-oil. Cyclopentadiene pyrolysis also produces compounds such as benzene, naphthalene and indene *via* C–C bond β-scission and C–H bond β-scission.[50] Cellulose pyrolysis results in the formation of cyclopentadienyl radicals and their combination *via* C–C bond β-scission to form benzene. Benzene reacts with cyclopentadienyl radicals *via* C–H bond β-scission to form naphthalene. The major polycyclic aromatic compounds present were 2-methyl naphthalene, 1,4,5-trimethyl naphthalene and 1,2-dihydro-6-methyl naphthalene. The wide spectrum of products obtained from the pyrolysis of USB imparts a reasonable idea about the complex structure of the SB biomass. Therefore, the conversions and interconversions necessary to understand the formation of important compounds become important. A detailed list of the compounds identified in the bio-oil from the pyrolysis of USB and PSB at different temperatures is provided in Table S1 (in the ESI†).

3.3.3. Composition of the bio-oil from the pyrolysis of PSB. Fig. 6 shows the variation in the different compounds present in the bio-oil obtained from the pyrolysis of PSB at different temperatures. The classification of the compounds was the same as that used for the bio-oil from USB. The amount of aliphatic hydrocarbons reduced as compared to bio-oil from USB. This reduction was due to the pre-treatment, as the presence of AAEM species inhibited the cracking reactions. The selectivity to aliphatic hydrocarbons in the bio-oil was as follows: 4.98% (800 °C) < 10.50% (600 °C) < 11.22% (700 °C). The lowest selectivity to aliphatic hydrocarbons was observed at 800 °C owing to the significant conversion of pyrolysis vapors into non-condensable gases as a result of high temperature cracking reactions. The selectivity to alkanes was found to be 2.70% and 2.45% at 600 and 700 °C, respectively from PSB, as compared to 4.52% and 5.16% at 600 and 700 °C, respectively from USB. The reduction in the selectivity to alkanes can be attributed to the reduced mineral content as minerals may assist in the formation of alkanes. The presence of alkali metals facilitated the formation of alkanes in the microalga species,

 This journal is © The Royal Society of Chemistry 2021

Open Access Article. Published on 26 February 2021. Downloaded on 7/28/2024 11:24:34 AM.
This article is licensed under a Creative Commons Attribution-NonCommercial 3.0 Unported Licence.

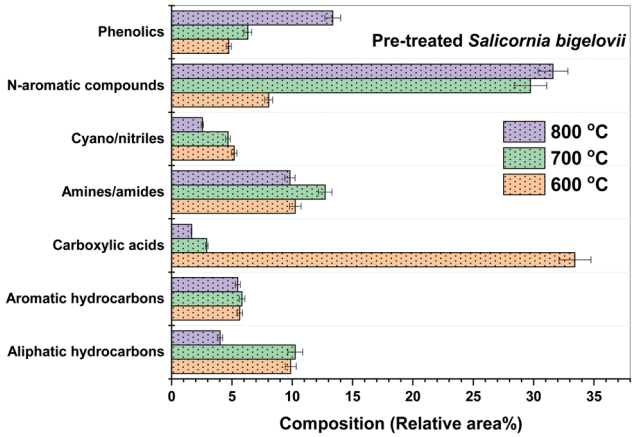

Fig. 6 Effect of temperature on the composition of bio-oil from the pyrolysis of PSB.

Nannochloropsis oculata.[41] The pre-treatment or ash removal did not alter the selectivities to alkenes and alkynes significantly. It is to be noted that the selectivity to long-chain hydrocarbons (≥C17) decreased significantly as compared to USB and the reduction was as follows: 23.6% (600 °C) < 57.1% (700 °C) < 90.1% (800 °C). From these observations, it can be inferred that the presence of AAEM species facilitated repolymerization reactions which increased with an increase in the temperature. Fig. S2a (in the ESI†) depicts the effect of temperature on the selectivity to hydrocarbons in the bio-oil from the pyrolysis of USB and PSB.

At 600 °C, the selectivity to carboxylic acids increased from 20.71% (USB) to 33.42% (PSB) in the bio-oil. At 600 °C, *n*-hexadecanoic acid (24.4%) was the major carboxylic acid along with linoleic acid (4.93%) and stearic acid (2.76%). The selectivity to carboxylic acids decreased significantly with the temperature as follows: 33.42% (600 °C) > 2.92% (700 °C) > 1.66% (800 °C). This can be attributed to the enhanced decarboxylation and cracking reactions. The presence of metals in the USB inhibited the extraction of carboxylic acids at 600 °C resulting in lower selectivity as compared to PSB. The removal of ash facilitated the extent of these reactions such as cracking and decarboxylation. Fig. S2b (in the ESI†) shows the effect of the temperature on the selectivity to the various oxygenated compounds in the bio-oil from the pyrolysis of USB and PSB. The major oxygenated compounds were classified as carbonyl compounds, esters and furan derivatives. As observed in the bio-oil from USB, the selectivity to the furan derivatives was as low as that observed in the bio-oil from PSB. These compounds did not have a significant variation in the bio-oil with either an increase in the temperature or pre-treatment of SB. The selectivity to furan derivatives was in the range of 1.6–1.9%. The selectivity to the esters in the bio-oil was significantly reduced by 30%, 60% and 70% at 600, 700 and 800 °C, respectively after the pre-treatment. The high selectivity to esters was a result of metals present in the ash in the USB. As the temperature increased, the selectivity to esters decreased from 5.17% at 600 °C to 1.87% and 1.58% at 700 and 800 °C, respectively. This reduction at higher temperatures can be attributed to the cracking of esters.

The bio-oil from the pyrolysis of PSB was found to be rich in nitrogen-containing compounds such as amines/amides, cyano/nitriles and nitrogen-containing heteroatomic aromatic compounds. This is a result of the high nitrogen content in PSB (4.65%) as compared to USB (2.8%) (Table 1). The selectivity to amides/amines increased from 10.25% at 600 °C to 13% at 700 °C and then reduced to 9.80% at 800 °C. This increment in amides from 600 to 700 °C can also be corroborated with the reduction in the selectivity to carboxylic acids as they react with ammonia evolved from the pyrolysis of amino acids. It can be inferred from this observation that the presence of AAEM species inhibited the reaction of carboxylic acids with ammonia, as the selectivity to amides from the pyrolysis of USB increased from 9.95% to 13% (PSB) at 700 °C. The major amide in the bio-oil was hexadecanamide, followed by 9-octadecenamide and octadecanamide. The dehydration of amides resulted in the formation of cyano/nitriles and their selectivity decreased as the temperature increased as follows: 5.19% (600 °C) > 4.68% (700 °C) > 2.55% (800 °C). Owing to the presence of minerals, the selectivity to nitriles from the pyrolysis of USB at 800 °C was higher (6.86%), compared to that from PSB (2.55%). This suggested the AAEM species present in SB facilitated the formation of cyano/nitriles compounds *via* dehydration reactions.

The bio-oil from the pyrolysis of PSB contained N-containing aromatics in significant amounts. The selectivity to these compounds followed the trend: 8.05% (600 °C) < 29.73% (700 °C) < 31.6% (800 °C). This can be attributed to the increased cyclization and aromatization reactions at a high pyrolysis temperature. Gautam and Vinu[41] also observed an increase in heteroatomic nitrogen containing aromatic compounds from the pyrolysis of protein-rich alga in response to the temperature. At 600 °C, 2-pyrrolidinone, 1H-indole, and β-carboline were found to be the most abundant compounds in the bio-oil. 5-(2-Methyl propyl)-2,4-imidazolidine, 5-ethyl-5-methyl-2,4-imidazolidine, 2-methylpyrazine, pyridine and 1,4,5-trimethyl imidazole were observed to be the major compounds at 700 °C. At 800 °C, 1H-indole, 3-pyridinol, 3-methyl-2,5-pyrrolidinedione, 2-aminopyridine and picolinamide were observed. The plausible conversion pathways for the formation of these compounds are depicted in Scheme 1.

Toluene (0.98–2.95%) was the major aromatic hydrocarbon identified in the bio-oil from the pyrolysis of PSB. The selectivity to polycyclic hydrocarbons, such as naphthalene derivatives, increased from 0.75% (600 °C) to 2.13% (700 °C). The formation of polycyclic compounds increases with an increase in the pyrolysis temperature. In the bio-oil from PSB, the selectivity to aromatic compounds was observed in the range 5.5–5.8% and no significant variations were observed. However, these selectivities were higher than those observed in the bio-oil from the pyrolysis of USB (2.8–4.6%). In addition to the aromatic compounds, the selectivity to phenolics increased in the bio-oil. The phenolics increased with the temperature as follows: 4.74% (600 °C) < 7.52% (700 °C) < 13.36% (800 °C). At all of the pyrolysis temperatures, phenol, *p*-cresol and another lignin derivative, guaiacol (2-methoxyphenol), were observed in the bio-oil from PSB.

Open Access Article. Published on 26 February 2021. Downloaded on 7/28/2024 11:24:34 AM.
This article is licensed under a Creative Commons Attribution-NonCommercial 3.0 Unported Licence.

The pre-treatment of the biomass did not significantly effect the conversion pathways, as observed from the compounds in the pyrolysis bio-oil (Table S1, in the ESI†). However, significant ash removal from the biomass enhanced the bio-oil yield, and, in addition, promoted the decarboxylation, cracking, aromatization and cyclization reactions. This resulted in the conversion of amino acids to heterocyclic nitrogen-containing aromatic compounds. The presence of AAEM species in significant amounts inhibited the extraction of the fatty acids in the bio-oil from the pyrolysis of USB. It is worth highlighting that the nitrogen-containing compounds, phenolics and aromatic hydrocarbons have several uses, for example, in pharmaceutical products, food preservatives, fuel additives and platform chemicals. The potential of the *Salicornia* biomass can be tapped efficiently by using catalysts to selectively produce these valuable platform chemicals. It is important to mention that the analysis of evolved gases during the pyrolysis of SB can certainly provide further insights into the decomposition mechanism. Therefore, this will be investigated as future work to gain a better understanding of the pyrolysis of the *Salicornia* biomass.

3.4. Characterization of biochar

3.4.1. Elemental analysis. Table 3 presents the properties of the biochar obtained from the pyrolysis of SB. USB 600, USB 700 and USB 800 represent the char obtained from the pyrolysis of untreated biomass at 600, 700, and 800 °C, respectively. A similar representation was used for the biochar obtained from the pyrolysis of PSB. The elemental analysis (C, H, N, S, O) and ash content of the different biochars are presented in Table 3. The carbon content of the biochar from the pyrolysis of USB and PSB was in the range of 47.9 to 50.6% and 47.1 to 48.8%, respectively. The carbon content in the different biochar samples was in a similar range. The hydrogen content in the biochar decreased as the pyrolysis temperature increased and the trends were as follows: 2.37% (USB600) > 1.47% (USB700) and 2.52% (PSB600) > 1.47% (PSB700). The oxygen content in the biochar from the pyrolysis of USB and PSB decreased with an increase in the temperature. The oxygen content decreased from 10.50% (600 °C) to 4.8% (700 °C) and then further decreased to 3.6% (800 °C) in the biochar from the pyrolysis of USB. The oxygen content was high in the biochar obtained from the pyrolysis of PSB and the following trend was observed: 31.20% (600 °C) > 28.66% (700 °C) > 20.6% (800 °C). This reduction in the hydrogen and oxygen content in the pyrolysis biochar can be attributed to the enhanced deoxygenation and dehydration reactions at high pyrolysis temperatures. The low oxygen content in the biochar from USB can be attributed to the high ash content. The nitrogen content in the char decreased with an increase in the temperature as the high temperature facilitates the release of nitrogen in the gas phase.

A Van Krevelen diagram (Fig. S3 in the ESI†) captures the transition from SB biomass to biochars obtained from the pyrolysis at different temperatures. The H/C ratios decrease significantly as compared to the feedstock. The H/C and O/C ratios decreased from 1.85 to 0.37, whereas the O/C ratio decreased from 0.63 to 0.06 in the case of the USB 800 biochar. For PSB, the H/C and O/C values were 1.73 and 0.42, respectively, which decreased to 0.37 and 0.33, respectively, for the PSB800 biochar. This decreasing trend slowed as the samples were pyrolyzed at higher temperatures. The reduction in these ratios with an increase in the pyrolysis temperature occurs due to the dehydration and decarboxylation reactions. The ratio of H/C is an indicator of the degree of carbonization: low values of this ratio indicate a high degree of unsaturation (number of bonds C=C) and aromaticity. It can be observed that at the same pyrolysis temperature, the demineralization treatment decreased the aromaticity and increased the polarity of the biochars, as indicated by the increasing atomic ratios of H/C and O/C in Table 3. It is important to mention that the biomass material typically consists of recalcitrant oxygen and a labile oxygen fraction.[51] During the initial heating this fraction is quickly lost, whereas the recalcitrant oxygen is left in the final product.

However, the O/C ratios offer information about the biochar stability and the degree of aromatization. If the O/C ratios of the biochar decrease, the stability increases. In fact, the aromatics are more stable when they show a minor oxygen percentage. Biochar is extensively recognized as a relatively stable form of C, owing to its prominent aromatic structure. At higher temperatures, the biochar from the untreated biomass has the lowest O/C, which indicates that the USB 800 biochar is more stable. This stability can be attributed to the presence of a large amount of aromatic organic matter.[52] At high temperatures, biochar has a low O/C ratio which is a result of the formation of an aromatic ring structure representing a stable crystal. These stable crystals resemble graphite-like structures. Biochar that has an O/C ratio of more than 0.6 has a half-life of less than 100 years, while an

Table 3 Properties of the biochar obtained from the pyrolysis of USB and PSB at different temperatures. Elemental analysis is reported in wt% (dry basis) and the data are reported as mean (S.D.), $n = 3$

	C (%)	H (%)	N (%)	O (%)	Ash (%)	H/C	O/C	pH	EC (mS cm^{-1})	Specific surface area (m^2 g^{-1})	Pore volume (cm^3 g^{-1})
USB600	49.23 (1.4)	2.37 (0.3)	6.60 (0.1)	10.50 (1.8)	31.3	0.57	0.16	10.06 (0.02)	23.80 (0.12)	2.23	0.007
PSB600	48.75 (1.3)	2.52 (0.2)	5.23 (0.2)	31.20 (1.7)	12.3	0.62	0.48	9.98 (0.1)	12.84 (0.75)	6.68	0.026
USB700	50.6 (0.8)	1.47 (0.3)	6.05 (0.1)	4.8 (1.2)	37.8	0.35	0.07	11.86 (0.07)	24.75 (0.21)	2.35	0.011
PSB700	47.27 (1.4)	1.47 (0.1)	5.6 (0.1)	28.66 (1.6)	17	0.37	0.45	11.27 (0.13)	16.13 (0.08)	7.94	0.026
USB800	47.90 (0.8)	1.50 (0.2)	5.22 (0.1)	3.6 (1.1)	41.8	0.37	0.06	11.44 (0.12)	30.4 (0.5)	1.30	0.001
PSB800	47.07 (0.7)	1.47 (0.2)	4.36 (0.1)	20.6 (0.8)	26.5	0.37	0.33	11.43 (0.06)	17.02 (0.1)	5.30	0.022

 This journal is © The Royal Society of Chemistry 2021

Open Access Article. Published on 26 February 2021. Downloaded on 7/28/2024 11:24:34 AM.
This article is licensed under a Creative Commons Attribution-NonCommercial 3.0 Unported Licence.

O/C ratio between 0.2 and 0.6 results in a half-life between 100 and 1000 years, and, finally, if it has a low O/C ratio (<0.2), it possesses a half-life of more than 1000 years.[53]

3.4.2. Mineral content. The mineral content of the biochar was determined using ICP-OES and the detailed ash composition was revealed. The ash content in the biochar increased as the temperature increased and the trend was found to be as follows: 31.3% (USB600) < 37.8% (USB700) < 41.8% (USB800). The trend for the ash content in the biochar obtained from the pyrolysis of PSB was: 12.3% (PSB600) < 17% (PSB700) < 26.5% (PSB800). This increase in the biochar can be attributed to a growing concentration of minerals and the progressive volatilization of lignocellulosic matters as the pyrolysis temperature increases.[53] The mineral composition of SB ascertained the presence of various elements such as Na, Mg, and Si with a minor amount of Al, Ca, and Fe. These metals individually increased in the biochar as the pyrolysis temperature increased. For example, the Na content in USB biochar increased with the temperature as follows: 12.6% (600 °C) < 12.8% (700 °C) < 13.57% (800 °C). The detailed composition of these metals in the ash is given in Table 4. There were less metals identified in the biochars obtained from the pyrolysis of PSB compared to the biochar from USB.

3.4.3. FTIR analysis of biochar. The FTIR spectra for the USB and biochar obtained from the pyrolysis of USB at different temperatures are depicted in Fig. 7. The different functional groups identified in the biochar are given in Table S2 (in the ESI†). The identification of different functional groups in the FTIR spectra of USB also confirmed the presence of lignin (phenols), amino acids (NH bends and stretching), and carboxylic acids (carbonyl group and C–H stretching) in the matrix of the biomass. The aliphatic C–H stretch is associated with the C–H stretching of methylene (–CH_2). The presence of the aromatic ring stretching and in- and out-of-plane bends can be attributed to the presence of the phenolic backbone of lignin and aromatic amino acids, such as phenylalanine. Similar vibrations were observed in the FTIR spectra of *Nannochloropsis oculata* owing to the presence of high amounts of proteins.[41] The presence of amino acids in the matrix of the biomass can be justified by the identification of the NH secondary amine, and the NH stretch and bend in the FTIR spectra of USB. The C–O and C–O–C bonds of the polysaccharides also contribute to the distinct band observed at 1030 cm^{-1}.

From Fig. 7, it can be observed that the functional groups in the residual char disappeared significantly. The disappearance

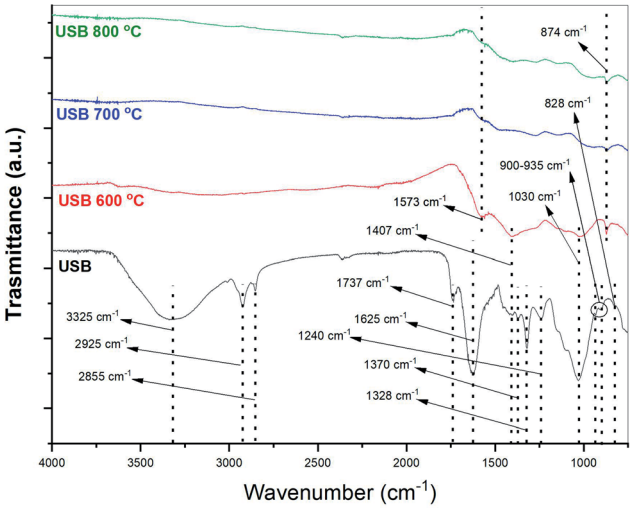

Fig. 7 FTIR spectra of the USB and pyrolysis biochar obtained at different temperatures.

of the broad O–H stretching in the FTIR spectra of biochar can be attributed to the dehydration reactions. However, a few peaks were observed in the spectra and they were primarily caused by the presence of aromatic structures in the biochar (874 cm^{-1}). This indicated the presence of polycyclic aromatic compounds which may be formed during the pyrolysis of carbon and hydrogen containing matter. The small peaks corresponding to the secondary amine bends at 1625 and 1573 cm^{-1} were seen in the FTIR spectra of the biochar, owing to the presence of nitrogen (Table 3). The peak at 1573 cm^{-1} disappeared as the pyrolysis temperature increased beyond 600 °C. This can be attributed to the deamination reactions of the amino acids present in the SB. Pyrolysis char from the microalgae model compounds had compounds such as 2,2-diphenyl-1-picrylhydrazyl and 3-nitrophthalic acid.[33] The presence of these compounds in the biochar strengthens the assertion that these heteroatomic polycyclic nitrogen-containing compounds are present in the biochar. It is also worthwhile mentioning that the FTIR spectra of biochar obtained from the pyrolysis of PSB were similar in terms of the identified peaks. Fig. S4 (in the ESI†) depicts a comparison of the FTIR spectra of raw biomass and biochar obtained from the pyrolysis of PSB at different temperatures. Dissolving the biochar in multiple solvents to determine the compounds will provide further insights into the formation of compounds in the biochar during the pyrolysis of SB.[33]

3.4.4. pH and electrical conductivity measurements of the biochars. The values of pH and electrical conductivity (EC) are shown in Table 3. The produced biochars were generally alkaline (pH > 7) and the pH values were found to increase with an increase in the pyrolysis temperature. This is due to the devolatilization of the acidic groups containing oxygen, such as decarboxylation and decarbonylation of the carboxyl and carbonyl groups, respectively. These reactions were enhanced as the temperature increased. As phenols are also weak acids, the reduction in the pH can be attributed to lignin deconstruction

Table 4 Mineral content of the biochar obtained from the pyrolysis of USB and PSB at different temperatures. The values are in wt% (dry basis)

	Al (%)	Ca (%)	Fe (%)	Mg (%)	Na (%)	Si (%)
USB600	0.40	0.30	0.45	1.80	12.60	0.98
PSB600	0.45	0.27	0.38	1.80	5.80	0.42
USB700	0.46	0.63	0.57	2.20	12.80	1.10
PSB700	0.57	0.30	0.46	1.43	6.10	0.53
USB800	0.57	0.65	0.62	2.50	13.57	1.15
PSB800	0.62	0.42	0.36	1.60	6.30	0.80

Open Access Article. Published on 26 February 2021. Downloaded on 7/28/2024 11:24:34 AM.
This article is licensed under a Creative Commons Attribution-NonCommercial 3.0 Unported Licence.

during the pyrolysis of SB. The pH value of biochar was obtained from the carbonization of SB at 350 °C for 6 h was 8.6.[54] This observation, obtained from previously published literature, clearly shows that the pH value of the biochar increases as the pyrolysis temperature increases. Furthermore, it was observed that the pre-treatment of SB did not affect the pH values of the biochar, irrespective of the temperature, and the pH values were between 10 and 11.86. Owing to the high alkalinity of biochars, they can be used for soil amendments, to increase soil pH and neutralize soil acidity.[55] More importantly, the application of pyrolysis biochar for soil amendments is strictly governed by environmental regulations imposed by different countries across the globe.

Table 3 shows that the values of EC increased with an increase in the temperature. The amount of metal content had an effect on the EC values of the biochar. This can be understood by the fact that the pre-treatment reduced the metal content and the biochar obtained from PSB had a lower EC as compared to USB. For example, at 800 °C, the EC values followed the trend: 30.4 mS cm^{-1} (USB) > 17.02 mS cm^{-1} (PSB). The mineral content values obtained from Table 4 can be translated to understand the trend in the EC values of the various biochars. The low EC values of the biochar may restrict their applications for the development of supercapacitors. The application of the biochar for fuel purposes ignores this aspect, in which electrical conductivity is irrelevant. Finally, from the above mentioned discussion, it was noticed that the ash content, mineral content, EC and pH correlated. Furthermore, as the temperature increased, the conductivity, ash content and pH increased.

3.4.5. Surface properties. In this section, the surface morphology, surface area, and pore size distribution are discussed. The BET adsorption isotherms of the biochars are provided in the ESI (Fig. S5†). The adsorption isotherms of the biochar obtained from the pyrolysis of USB and PSB were qualitatively similar at all the pyrolysis temperatures. The isotherms were observed to have a high and low-pressure hysteresis as a result of the non-elasticity of the material. The precise determination of the pore size distribution becomes difficult owing to hysteresis. As per the IUPAC classification, the form of the adsorption isotherm is typical of type II isotherms that are obtained in the case of a non-porous or macroporous solids. The knee of the isotherm indicates the stage at which an adsorbate monolayer covers the surface of the material. For higher partial pressures, multilayer adsorption occurs. The BET surface area and pore volume of the biochar samples are given in Table 3.

Biochars from PSB have slightly higher values as compared to USB. The high surface area of the biochars from PSB can be attributed to the less inhibited pyrolysis resulting from the removal of the metals from the matrix of the biomass. The specific surface area of the biochar samples from the pyrolysis of USB and PSB was in the range 1.30–2.35 and 5.33–7.94 m^2 g^{-1}, respectively. The low lignin content (2–10%) reported for the SB biomass may have resulted in the low surface area of the biochar.[44] Marzooqi *et al.*[54] also observed the low BET surface area (1.72 m^2 g^{-1}) of the biochar from SB. In fact, the low structural stability during the charring process can be attributed to this small amount of lignin in the biomass. The high salt content in the SB biomass can also be held responsible for these low surface area values as the salt concentration (in ash) in USB might have clogged the pores. In a recent study by Wei *et al.*,[56] the BET surface area of the biochar obtained from the pyrolysis of a low ash containing halophyte, Jerusalem artichoke stalks, was in the range of 7–8.5 m^2 g^{-1}. It can be concluded that the ash content has a direct effect on the surface area of the pyrolysis biochar.

The surface areas of the biochar samples from both USB and PSB first increased as the temperature increased from 600 to 700 °C, and then decreased considerably at 800 °C. Pyrolysis of the biomass results in the decomposition and condensation of the biochemical constituents leading to the formation of pores. The change in the pyrolysis temperature changes the surface morphology and surface area. Above 700 °C, the pore structures collapsed and resulted in the reduced specific surface area at higher temperatures. A similar trend was observed in the previously published literature by Irfan *et al.*,[19] who reported the low surface areas of the biochar from the pyrolysis of halophyte grass, *Achnatherum splendens* L. The surface area increased from 7.03 m^2 g^{-1} (300 °C) to 12.56 m^2 g^{-1} (500 °C) and then decreased to 5.24 m^2 g^{-1} (700 °C). A detailed review by Tomczyk *et al.*,[57] that aimed to discuss the physicochemical properties of biochars from various biomasses, was published recently. It is worthwhile mentioning that the use of the biochars from the pyrolysis of the halophyte species has shown promising results for the adsorption of toxic metals and to stimulate the biological activity of the soil.[54,56] This suggests that the pyrolysis biochar from SB has a good potential for use in future research involving adsorption and soil amendment.

The surface morphology of the biochar was revealed using SEM images of the biochar. Fig. 8a and b depict the SEM images of the biochar obtained from the pyrolysis of USB and PSB, respectively at 800 °C. Fig. 8a clearly shows the holes and the relatively large cylindrical tube-like structures. This can be attributed to the formation of nanostructures in the biochar. Recently, Osman *et al.*[58] used *Miscanthus* grass, lignocellulosic biomass rich in alkali silicates to produce carbon nanomaterials *via* pyrolysis. In another study by Bernd *et al.*,[59] carbon nanostructures were produced by pyrolyzing wood sawdust at similar pyrolysis temperatures (750 °C) in a tubular reactor. It can be inferred that the presence of alkali metals in the matrix of the SB aided in the formation of carbon nanostructures on the surface of the biochar. The opening of holes on the surface of the biochar from PSB is evident from Fig. 8b. The opening of these holes increased the specific surface area of the biochar from PSB by more than four times (from 1.30 to 5.55 m^2 g^{-1}) as compared to USB. The pore volume of the biochar also increased to 0.022 cm^3 g^{-1} (PSB) from 0.001 cm^3 g^{-1} (USB). The AAEM species in USB also restricted the opening of the pores on the biochar. It can be seen from Fig. 8a that the tube-like structures were sparsely distributed, which is also corroborated by the low specific surface area. From the point of view of future research, various techniques, such as acid pre-treatment and chemical activation prior to pyrolysis, can be used for

 This journal is © The Royal Society of Chemistry 2021

Open Access Article. Published on 26 February 2021. Downloaded on 7/28/2024 11:24:34 AM.
This article is licensed under a Creative Commons Attribution-NonCommercial 3.0 Unported Licence.

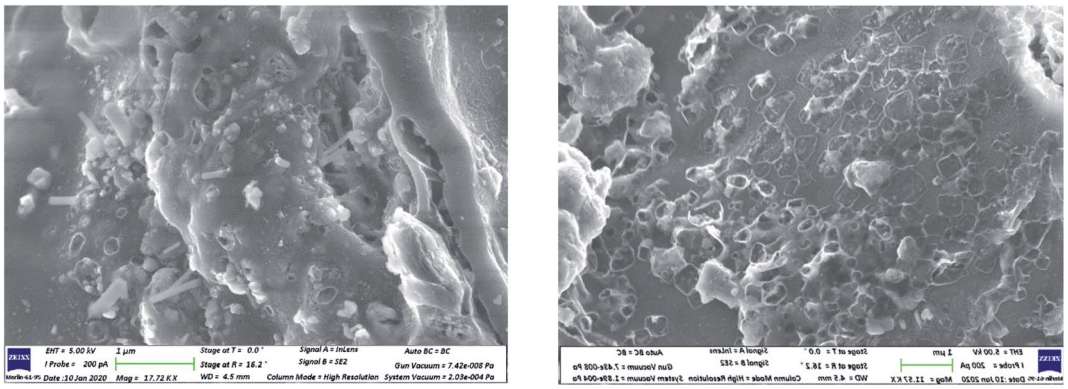

Fig. 8 SEM images of the biochar obtained from the pyrolysis of (a) USB and (b) PSB at 800 °C.

opening the pores of the raw SB biomass, which in turn can produce a biochar rich in carbon nanostructures.

4. Conclusions

This study presents the effects of incorporating a water-washing pre-treatment on the product yields from the pyrolysis of *Salicornia bigelovii*. The optimum pyrolysis temperature for the bio-oil production was 700 °C. The bio-oil yields from PSB were 25% higher as compared to the bio-oil yield from USB at 600 and 700 °C. The GC/MS analysis of bio-oil revealed that the degradation of SB occurred *via* reactions such as dehydration, decarboxylation, decarbonylation, deamination, amination, aromatization, and cyclization. In the bio-oil obtained from the pyrolysis of USB, carboxylic acids (10–21%) and N-aromatic compounds (12–18%) were the major products. Whereas, in the bio-oil from the pyrolysis of PSB, carboxylic acids (33%) were the major products at 600 °C and N-aromatic compounds were the major products at 700 °C (29.7%) and 800 °C (31.6%). The presence of AAEM species in SB had an inhibiting effect for the majority of the reactions occurring during pyrolysis. The highest biochar yield was observed at 600 °C (45.7%) from the pyrolysis of USB, which reduced to 36.7% from the pyrolysis of PSB. It was also revealed that the pre-treatment of SB resulted in the opening of the pores in the pyrolysis biochar, whereas the biochar from USB exhibited the presence of carbon nanostructures on its surface. This pre-treatment step provides a basis to evaluate alternatives such as acid-washing and chemical activation to enhance the product yields. The selective production of valuable chemicals *via* catalysis and obtaining carbon nanostructure rich pyrolysis biochar should be investigated further in the future.

Author contributions

Alessia Iaccarnio: conceptualization, methodology, formal analysis, visualization, writing – original draft. Ribhu Gautam: formal analysis, visualization, writing – original draft, writing – review & editing. S. Mani Sarathy: conceptualization, methodology, formal analysis, visualization, writing – original draft, writing – review & editing, resources, supervision.

Conflicts of interest

The authors declare that they have no known competing financial interests or personal relationships that could have appeared to influence the work reported in this paper.

Acknowledgements

This work was sponsored by King Abdullah University of Science and Technology (KAUST). AI acknowledges support from the KAUST Visiting Student Research Program (VSRP). We thank Mark Tester, Muppala Reddy, Gabriele Fiene, and Octavio Salazar Moya from the KAUST Center for Desert Agriculture for providing the biomass samples.

References

1 D. Gielen, F. Boshell, D. Saygin, M. D. Brazilian, N. Wanger and R. Gorini, *Energy Strategy Rev.*, 2019, **24**, 38–50.
2 C. Liu, H. Wang, A. M. Karim, J. Sun and Y. Wang, *Chem. Soc. Rev.*, 2014, **43**, 7594–7623.
3 S. K. Bardhan, S. Gupta, M. E. Gorman and M. A. Haider, *Renewable Sustainable Energy Rev.*, 2015, **51**, 506–520.
4 M. C. Rulli, D. Bellomi, A. Cazolli, G. D. Carolis and P. D'Odorico, *Sci. Rep.*, 2016, **6**, 22521.
5 H. A. Alawan, A. H. Alminshid and H. A. S. Aljaafari, *Renew. Energy Focus*, 2019, **28**, 127–139.
6 M. S. Hossain, *Int. J. Biol. Sci.*, 2019, **1**, 1–3.
7 T. J. Flowers and T. D. Colmer, *New Phytol.*, 2018, **179**, 945–963.
8 R. Sharma, S. Wungrampha, V. Singh, A. Pareek and M. Sharma, *Front. Plant Sci.*, 2016, **7**, 1372.
9 K. A. El-Tarabily, A. S. AlKhajeh, M. M. Ayyash, L. H. Alnuaimi, A. Sham, K. Z. ElBaghdady, S. Tariq and S. F. AbuQamar, *Front. Microbiol.*, 2019, **10**, 1694.
10 Y. Kong and Y. Zheng, *Hortic. Sci.*, 2014, **49**, 1154–1157.

Open Access Article. Published on 26 February 2021. Downloaded on 7/28/2024 11:24:34 AM.
This article is licensed under a Creative Commons Attribution-NonCommercial 3.0 Unported Licence.

11 V. R. Squires, *Range and animal sciences and resources management – volume I*, ELOSS Publications, Oxford, 2010.
12 D. W. Rains, in *The Biosaline Concept*, ed. A. Hollaender, J. C. Aller, E.Epstein, A. S. Pietro and O. R. Zaborsky, Plenum Press, New York, 1st edn, 1979, vol. 14, ch. 3, pp. 47–67.
13 Salicornia-Project_Brief-Final-2. Pdf, https://www.biosaline.org/sites/default/files/Projectbrieffiles/Salicornia-Project_Brief-Final-2.pdf, 2020, accessed November 2020.
14 ICBA achieves progress in breaking Salicornia yield ceiling, http://biosaline.org/news/2018-05-10-6466, accessed November 2020.
15 M. Shahid and N. K. Rao, *Biosalinity News*, 2011, **12**, 6.
16 A. J. Folayan, P. A. L. Anawe and A. O. Ayeni, *Cogent. Eng.*, 2019, **6**, 1625847.
17 J. W. Lee, B. Hawkins, D. M. Day and D. C. Reicosky, *Energy Environ. Sci.*, 2010, **3**, 1695–1705.
18 R. Gautam and R. Vinu, *React. Chem. Eng.*, 2020, **5**, 1320–1373.
19 M. Irfan, Q. Chen, Y. Yue, R. Pang, Q. Lin, X. Zhao and H. Chen, *Bioresour. Technol.*, 2016, **211**, 457–463.
20 K. A. A. AlShareef and L. Ali, *Bioresour. Technol. Rep.*, 2020, **12**, 100577.
21 P. Dzidzienyo, J. Bastidas-Oyanedel and J. E. Schmidt, *Energies*, 2018, **11**, 2283–2290.
22 L. Li, X. Wang, J. Sun, Y. Zhang and S. Qin, *BioMed Res. Int.*, 2013, **2013**, 162907.
23 ASTM E1131-08, Standard test method for compositional analysis by thermogravimetry, https://www.astm.org/Standards/E1131.htm, accessed Nov 2020.
24 L. Deng, T. Zhang and D. Che, *Fuel Process. Technol.*, 2013, **106**, 712–720.
25 C. D. Blasi, C. Branca and G. D'Errico, *Thermochim. Acta*, 2000, **364**, 133–142.
26 K. Cen, J. Zhang, Z. Ma, D. Chen, J. Zhou and H. Ma, *Bioresour. Technol.*, 2019, **278**, 26–33.
27 D. Chen, Y. Wang, Y. Liu, K. Cen, X. Cao, Z. Ma and Y. Li, *Fuel*, 2019, **252**, 1–9.
28 R. Kumar, V. Strezov, H. Weldikidan, J. He, S. Singh, T. kan and B. Dastjerdi, *Renewable Sustainable Energy Rev.*, 2020, **123**, 109763.
29 J. N. Putro, F. E. Soetaredjo, S. Lin, Y. Ju and S. Ismadji, *RSC Adv.*, 2016, **6**, 46834–46852.
30 R. K. Mishra and K. Mohanty, *Bioresour. Technol.*, 2018, **251**, 63–74.
31 L. Gašparovič, Z. Koreňová and Ľ. Jelemenský, *Chem. Pap.*, 2010, **64**, 174–181.
32 F. M. Attia, A. A. Alsobayel, M. S. Kriadees, M. Y. Al-Saiady and M. S. Bayoumi, *Anim. Feed Sci. Technol.*, 1997, **65**, 257–263.
33 R. Gautam and R. Vinu, *React. Chem. Eng.*, 2019, **4**, 278–297.
34 H. Yang, R. Yan, H. Chen, D. H. Lee and C. Zheng, *Fuel*, 2007, **86**, 1781–1788.
35 W. R. Livingston, *Biomass ash characteristics and behavior in combustion, gasification and pyrolysis systems*, Doosan Babcock Energy Limited, West Sussex, U.K., 2007.
36 P. R. Patwardhan, J. A. Satrio, R. C. Brown and B. H. Shanks, *Bioresour. Technol.*, 2010, **101**, 4646–4655.
37 J. Lalak, D. Martyniak, A. Kasprzycka, G. Żurek, W. Moroń, M. Chmielewska, D. Wiącek and J. Tys, *Int. Agrophys.*, 2016, **30**, 475–482.
38 G. E. Parks, M. A. Dietrich and K. S. Schumaker, *J. Exp. Bot.*, 2002, **53**, 1055–1065.
39 R. W. Bryers, *Prog. Energy Combust. Sci.*, 1996, **22**, 29–120.
40 R. K. Mishra and K. Mohanty, *J. Anal. Appl. Pyrolysis*, 2018, **134**, 83–92.
41 R. Gautam and R. Vinu, *Algal Res.*, 2018, **34**, 12–24.
42 H. Persson and W. Wang, *Fuel*, 2019, **252**, 200–209.
43 A. Zheng, Z. Zhao, S. Chang, Z. Huang, H. Wu, X. Wang, F. He and H. Li, *J. Mol. Catal. A: Chem.*, 2014, **383–384**, 23–30.
44 S. D. Stefanidis, E. Heracleous, D. T. Patiaka, K. G. Kalogiannis, C. M. Michailof and A. A. Lappas, *Biomass Bioenergy*, 2015, **83**, 105–115.
45 J. A. Bañuelos, I. Velázquez-Hernández, M. Guerra-Balcazar and N. Arjona, *Renewable Energy*, 2018, **123**, 125–134.
46 R. Gautam, S. Shyam and R. Vinu, *Sustainable Energy Fuels*, 2019, **3**, 3009–3020.
47 S. C. Moldoveanu, *Analytical Pyrolysis of Natural Organic Polymers*, Elsevier, 1998.
48 C. Zhao, E. Jiang and A. Chen, *J. Energy Inst.*, 2017, **90**, 902–913.
49 G. Jiang, D. J. Nowakowski and A. V. Bridgwater, *Energy Fuels*, 2010, **24**, 4470–4475.
50 D. Wang, A. Violi, D. H. Kim and A. Mullholland, *J. Phys. Chem. A*, 2016, **110**, 4719–4725.
51 D. W. Rutherford, R. L. Wershaw, C. E. Rostad and C. N. Kelly, *Biomass Bioenergy*, 2012, **46**, 693–701.
52 K. Jindo, H. Mizumoto, Y. Sawada and T. Sonoki, *Biogeosciences*, 2011, **11**, 6613–6621.
53 K. Spokas, *Carbon Manag.*, 2010, **1**, 289–303.
54 F. A. Marzooqi and L. F. Yousef, *Appl. Soil Ecol.*, 2017, **114**, 9–15.
55 Q. Wan, J. Yuan, R. Xu and X. Li, *Environ. Sci. Pollut. Res.*, 2014, **21**, 2486–2495.
56 J. Wei, C. Tu, G. Yuan, Y. Lin, D. Bi, L. Xiao, J. Lu, B. K. G. Theng, H. Wang, L. Zhang and X. Zhang, *Environ. Pollut.*, 2019, **251**, 56–65.
57 A. Tomczyk, Z. Sokołowska and P. Boguta, *Rev. Environ. Sci. Bio/Technol.*, 2020, **19**, 191–215.
58 A. I. Osman, C. Farrell, A. H. Al-Muhtaseb, J. Harrison and D. W. Rooney, *Sci. Rep.*, 2018, **10**, 2563.
59 M. G. S. Bernd, S. R. Bragança, N. Heck and L. C. P. D. Filho, *J. Mater. Res. Technol.*, 2017, **6**, 171–177.

 This journal is © The Royal Society of Chemistry 2021